Large magnetostriction of $Fe_{1-x}Ge_x$ and its electronic origin: Density functional study

J. X. Cao, Y. N. Zhang, W. J. Ouyang, and R. Q. Wu
Department of Physics and Astronomy, University of California, Irvine, California 92697, USA
(Received 21 May 2009; published 14 September 2009)

The magnetostriction of $Fe_{1-x}Ge_x$ with $x \leq 25\%$ has been investigated with the density functional all-electron full-potential-linearized augmented plane wave method. It was found that at low concentration the magnetostriction linearly increases with x, because of elimination of Fe-Fe bonds. When Fe atoms get two or more Ge neighbors, starting from $x=11\%$, the magnetostriction rapidly decreases and gradually becomes negative at $x=14\%$ along with the development of the DO_3 structure. The spin-orbit coupling interactions among states localized at Fe atoms nearest to Ge are crucial. In particular, the availability of e_g holes above the Fermi level leads to the negative magnetostriction.

DOI: 10.1103/PhysRevB.80.104414 PACS number(s): 75.80.+q, 71.20.Be, 75.30.Gw, 75.50.Bb

I. INTRODUCTION

Highly magnetostrictive materials are important for broad applications such as sensor, transducer, and Micro Electro Mechanical Systems (MEMS).[1] Although rare-earth 3*d* transition metal compounds such as Terfenol-D have large magnetostriction, their use was somewhat limited by the need of high-saturation magnetic field and brittleness.[2,3] A new category of magnetostrictive materials has been developed based on Fe, mixed with nonmagnetic elements such as Ga,[4,5] Al,[6] Zn, Ge,[7–9] and Be.[10,11] In particular, it was found that tetragonal magnetostrictive coefficient (λ_{001}) of $Fe_{1-x}Ga_x$ (Galfenol) increases almost quadratically with the Ga concentration and may achieve to as large as 400 ppm at $x=17-20$ %.[3,12,13] Even stronger magnetostriction, with $\lambda_{001} > 1100$ ppm, has been reported recently for melt-spun $Fe_{1-x}Ga_x$ ribbons,[14,15] about 20–50 times larger than that of pure Fe. Furthermore, the $\lambda_{001}(x)$ curve of Galfenol displays a second high maximum after a sharp dip at $x = \sim 23-25$ %.[16] Along with their excellent ductility, Galfenol and related alloys are very promising smart materials for various applications.

The explanation for the extraordinary magnetostrictive behavior of Galfenol and related alloys is still developing. Based on the measured elastic constants, the origin of high magnetostriction of $Fe_{1-x}Ga_x$ can be partially attributed to lattice softening due to the presence of Ga.[13] However, the importance of distribution of Ga has been increasingly recognized, from the noticeable difference between λ_{001} of annealed and rapidly quenched samples. It was demonstrated through density functional calculations that the sign and magnitude of λ_{001} of Galfenol strongly depend on the arrangement of Ga atoms.[17] The B2-like structure, with a Ga-Ga distance of ~3 Å, was found to be essential for the establishment of large positive λ_{001}. Indeed, recent extended x-ray absorption fine structure measurements observed a high percentage of B2-like Ga-Ga pairs[18] and they mediate the magnetostriction by inducing large strains in Ga-Fe bonds.[19] The extrinsic effects of nanoscale precipitations on magnetostriction were also discussed recently.[20,21]

To reveal the mechanism of the striking enhancement of λ_{001} of Galfenol and, furthermore, to guide the design of high performance smart materials, it is constructive to study the effect of other elements such as Al, Zn, Be, and Ge. Among related alloys, $Fe_{1-x}Ge_x$ has a relatively simple phase diagram and it adopts the DO_3 structure in a broad composition range. Therefore, this system is more suitable for extensive density functional calculations for the studies of electronic origin of large magnetostriction. In contrast to the double peak structure of the $\lambda_{001}(x)$ curve of Galfenol, λ_{001} of $Fe_{1-x}Ge_x$ drops monotonically after $x > 11\%$ and becomes negative at $x=14.5\%$. In this paper, we report results of structural, magnetic, and magnetoelastic properties of $Fe_{1-x}Ge_x$ alloys with $x \leq 25\%$, obtained through systematic density functional calculations. After a brief discussion in computational details in Sec. II, we will provide the calculated magnetostrictive coefficients of $Fe_{1-x}Ge_x$ alloys and elucidate the electronic origin.

II. COMPUTATIONAL DETAILS

We used the all-electron full-potential-linearized augmented plane wave (FLAPW) method,[22,23] along with the generalized gradient approximation (GGA) in the formula of Perdew-Burke-Ernzerhof[24] for the description of exchange-correlation interaction. No shape approximation was assumed in charge, potential, and wave-function expansions. Energy cutoffs of 225 and 16 Ry were chosen for the charge potential and basis expansions in the interstitial region. Spherical harmonics with a maximum angular momentum quantum number of $l_{max}=8$ were used in the muffin-tin spheres ($r_{Fe}=1.11$ Å and $r_{Ge}=1.16$ Å). The $2\times2\times2$ and $3\times3\times3$ cubic supercells that comprise either 16 or 54 atoms were chosen to simulate $Fe_{1-x}Ge_x$ alloys. The lattice constants and atomic positions were optimized through the energy-minimization procedure, guided by calculated forces. We used 550 and 196 k points in the irreducible Brillouin zone for the $2\times2\times2$ and $3\times3\times3$ supercells, respectively.

The torque approach[25] was adopted for the determination of strain dependence of magnetic anisotropy energies, $E_{MCA}(\varepsilon)$. The magnetostrictive coefficients were calculated with[26]

$$\lambda = \frac{2}{3}\frac{dE_{MCA}/d\varepsilon}{d^2E_{tot}/d\varepsilon^2}, \quad (1)$$

where E_{tot} is the total energy. The tetragonal magnetostrictive coefficients, λ_{001}, were determined with the constant-

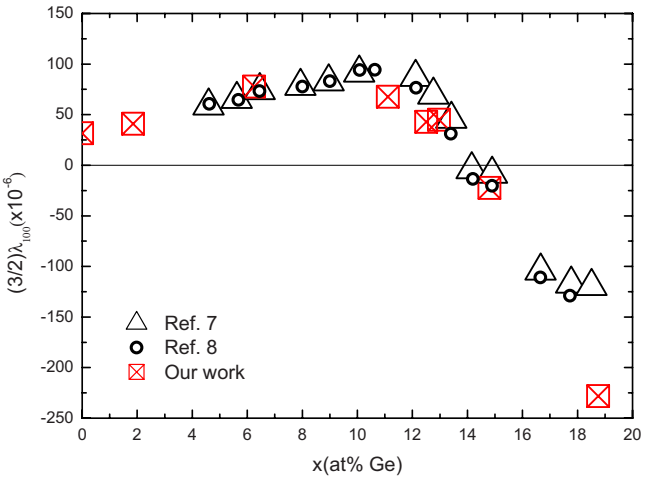

FIG. 1. (Color online) The calculated concentration dependence of magnetostriction of $Fe_{1-x}Ge_x$ alloys, with the most stable atomic arrangement for each x. Experimental results were taken from Refs. 7 and 8.

volume distortion mode ($\varepsilon_x=\varepsilon_y=-\varepsilon/2$ and $\varepsilon_z=\varepsilon$). The numerator $dE_{MCA}/d\varepsilon$ and denominator $d^2E_{tot}/d\varepsilon^2$ in Eq. (1) associate with magnetoelastic constant b_1 and the tetragonal shear modulus c' as,

$$-b_1=\frac{2}{3V_0}\frac{dE_{MCA}}{d\varepsilon} \quad \text{and} \quad c'=\frac{1}{3V_0}\frac{d^2E_{tot}}{d\varepsilon^2}. \tag{2}$$

Here V_0 is volume of the unit cell. From Eqs. (1) and (2), one can easily get

$$\lambda_{100}=-\frac{b_1}{3c'}. \tag{3}$$

III. RESULTS AND DISCUSSIONS

Since the arrangement of Ge is unknown, we explored several configurations for each x value, including some fcc-type structures. As a result, the bcc-type structures are preferred for $Fe_{1-x}Ge_x$ in the entire range of x we studied here. Using the most stable structure for every x value, the concentration dependence of magnetostriction is shown in Fig. 1. For comparison, the experimental data measured by Wu *et al.*[7] and Petculescu *et al.*[8] are also shown. The agreement between theory and experiment is excellent, especially under the condition that the small magnitude of λ_{001} is in the order of $10^{-5}-10^{-4}$. On the other hand, it is clear that the structures we determined from total energies appropriately represent those in real samples. In these structures, there is no first or even second-neighboring Ge pair and the shortest Ge-Ge distance is $\sqrt{2}a$, as in the DO_3 structure. This is in line with the phase diagram[27,28] of $Fe_{1-x}Ge_x$ alloys and experimental observations,[7,8] both indicate that the DO_3 phase develops from $x=16\%$. The magnetostriction increases linearly with the Ge concentration up to $x=11\%$ to a maximum value of 72 ppm; and then drops rapidly with further addition of Ge. Using the ground state DO_3-like geometries, our calculated values of λ_{001} are −164 and −730 ppm of $Fe_{1-x}Ge_x$ with $x=18.5\%$ and 25%, respectively.

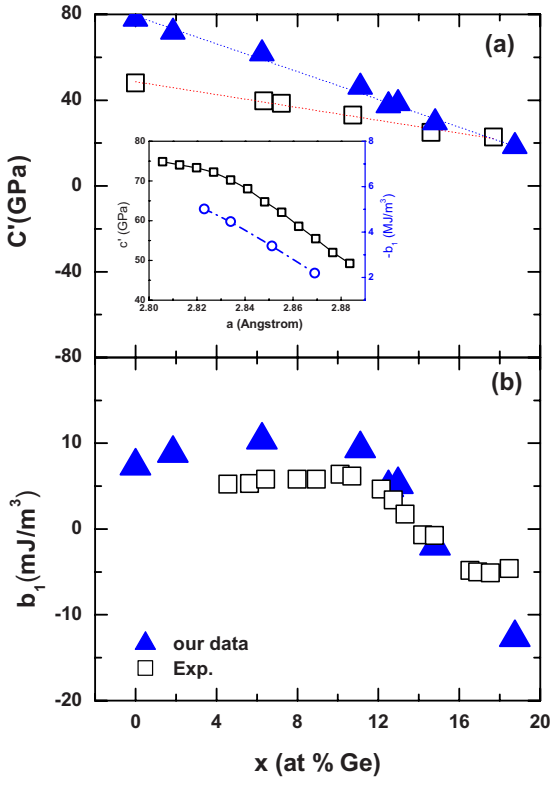

FIG. 2. (Color online) The calculated (a) tetragonal shear modulus and (b) magnetoelastic constant of $Fe_{1-x}Ge_x$ alloys at different x. The inset shows the calculated tetragonal shear modules and magnetoelastic constants for the bulk bcc Fe with different lattice constants.

It is instructive to separately analyze the contributions from magnetoelasticity and tetragonal shear modulus toward magnetostriction. We plot curves of $c'(x)$ and $b_1(x)$ in Fig. 2, together with the corresponding experimental data. Apparently, density functional calculations reproduces the experimental trends of both c' and b_1, but their magnitudes are somewhat overestimated. It was found that the deviations associate with the underestimation of the lattice sizes of $3d$ elements, a known deficiency of GGA. As displayed in the insets of Fig. 2(a), one can see that the calculated lattice constant of Fe is about 1.5% smaller than the experimental value. On the other hand, both $c'(x)$ and $b_1(x)$ are sensitive to the lattice constants. If the experimental lattice size is used, we get 54 GPa and 2.1 MJ/m^3 for c' and b_1 for the bulk bcc Fe, in good accordance with experimental data.[29] Nevertheless, the magnetostriction is almost independent of the lattice constant due to the mutual cancellation between errors for $c'(x)$ and $b_1(x)$ as expressed in Eq. (3). When the Ge concentration increases to about 20%, the optimized lattice constant is almost the same as the experimental value and the agreement for $c'(x)$ and $b_1(x)$ is significantly improved.

In Fig. 2, it is obvious that the enhancement of magnetostriction at small x mainly results from the softening of shear modulus. The value of b_1 also gradually increases with x but suddenly drops at $x=11\%$. As was discussed for $Fe_{1-x}Be_x$ in Ref. 11, the increase in $b_1(x)$ for $x<11\%$ can be attributed to two factors. First, the presence of Ge or other metalloid im-

TABLE I. The calculated lattice constants (in Å), total energy difference from the ground-state DO_3 structure (E_{diff}, in meV per Fe_3Ge unit), C' (in GPa), C_{44} (in GPa), and λ_{001} (in ppm) for $Fe_{0.75}Ge_{0.25}$ in different structures.

Configuration	a and c	E_{diff}	C'	C_{44}	λ_{001}
DO_3	a=5.71	0.00	6.8	130	−730
$L1_2$	a=7.27	98	14.2	104	+457
B2-like	a=5.64, c=5.84	267	17.2	110	−182
Cubic	a=5.73	371	15.4	102	−250

purities eliminates the nearest Fe-Fe bonds and therefore the density of states around the Fermi level increases. The availability of nonbonding Fe d states across the Fermi level enhances the spin-orbit coupling interaction between the occupied and unoccupied states and hence leads to stronger magnetoelastic coupling. Meanwhile, metalloid impurities transfer electrons to the surrounding Fe atoms and, as a result, the occupancy of Fe d bands increases with x. From the rigid band model analysis [cf. Fig. 5(b) in Ref. 11], the magnitude of magnetoelastic constant b_1 of Fe should also increase accordingly.

For $x>11\%$, Fe atoms start having two Ge neighbors[30] and their electronic structures are significantly affected. The arrangement of the two Ge atoms around Fe becomes an important issue, reflected from the sensitivity of magnetoelastic coupling to the change in ordered structures for $Fe_{0.75}Ge_{0.25}$ shown in Table I and Fig. 3. Among all atomic structures, the DO_3 structure is the most stable one, as expected from the phase diagram. As shown in Fig. 3, we found that only the $L1_2$ structure gives positive magnetostriction, i.e., $dE_{MCA}/d\varepsilon>0$. In contrast, all structures that have the bcc lattice give negative magnetostriction. Experimentally,[7,8] it was confirmed that $Fe_{1-x}Ge_x$ has negative λ_{001} for $x<14\%$ and the structures stay in the bcc-type lattice. Obviously, the magnetostriction of $Fe_{1-x}Ge_x$ is dominated by the behavior of b_1 for $x>11\%$.

Careful analyses suggest that the spin-orbit coupling interactions among states localized at Fe atoms nearest to Ge (denoted as Fe_1 below) play the key role, with about 80% contributions toward E_{MCA}. From the projected density of states (PDOSs) of the t_{2g} and e_g orbitals of Fe_1 in Fig. 4, one can find several remarkable features. (1) The exchange splitting between e_g states in two spin channels shrinks with the increase in x. (2) The density of nonbonding states, manifested by high peaks in the PDOS curves around the Fermi level, increases with x. (3) Electrons transfer from the e_g to the t_{2g} state, particularly in the majority spin channel. The t_{2g} holes for the pure Fe gradually disappear whereas e_g hole

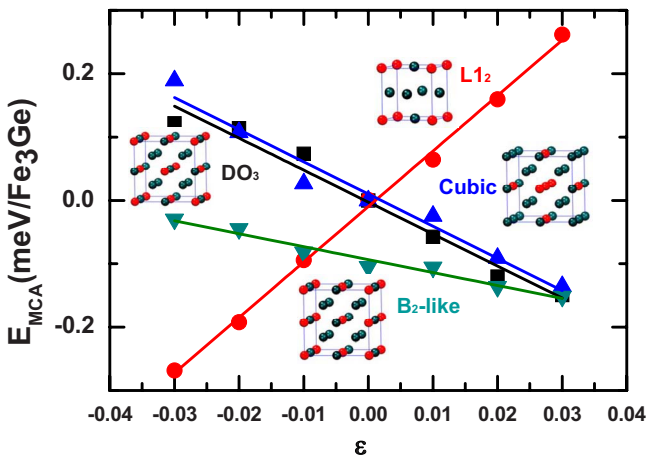

FIG. 3. (Color online) Strain dependence of E_{MCA} of $Fe_{0.75}Ge_{0.25}$ in different atomic structures.

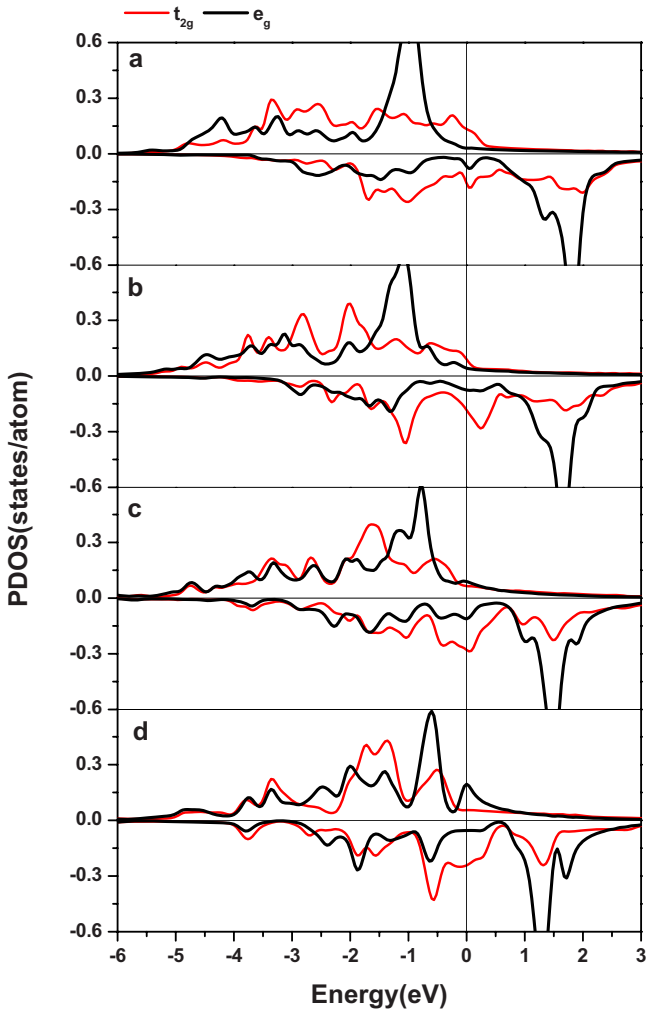

FIG. 4. (Color online) The projected density of states for t_{2g} and e_g orbitals of the Fe_1 atom in $Fe_{1-x}Ge_x$ with (a) x=0.0625; (b) 0.125; (c) 0.1875; and (d) 0.25. Zero energy indicates the position of the Fermi level.

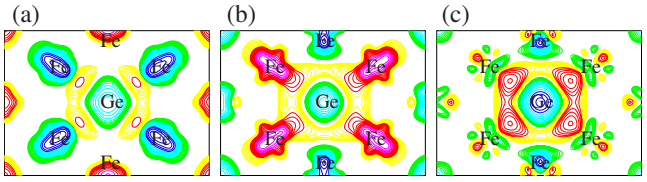

FIG. 5. (Color online) Charge-density differences for $Fe_{0.9375}Ge_{0.0625}$ in (a) majority spin part, (b) minority spin part, and (c) total charge. Yellow, red, and pink (light gray) are for charge accumulation whereas green, cyan, and blue (dark gray) are for charge depletion. Contours start from 2.0×10^{-5} e/Å^3 and increase consecutively by a factor of 1.2.

develops. There is even a small e_g peak right at the Fermi level for the $Fe_{0.75}Ge_{0.25}$ alloy in its DO_3 ground-state geometry. As a result, large negative magnetostriction is produced through the negative contribution $\langle z^2|L_x|xz,yz\rangle$ toward the anisotropy energy in responding to the tetragonal strain[31] in the majority spin channel. For example, the contributions from spin-orbit coupling through up-up, up-down, and down-down channels are −0.4, 0.19, and −0.08 for DO_3 $Fe_{0.75}Ge_{0.25}$ alloy under a strain $\varepsilon=0.03$, respectively. Interestingly, the up-up contribution is minimal for cases with low Ge concentrations, for which there is no e_g state above the Fermi level as seen in panels (a) and (b) of Fig. 4.

To better appreciate the charge redistribution in $Fe_{1-x}Ge_x$, we show the charge-density difference defined as ρ_{FeGe}-ρ_{Fe}-ρ_{Ge} where ρ_{Fe} and ρ_{Ge} are charge densities of reference systems for $x=0.0625$. The total charge redistribution around Ge in Fig. 5(c) is phenomenal, characterized by charge depletion from Ge and accumulation between the nearest Fe-Ge bonds. Further splitting into two separate spin channels indicates that the Fe_1 atoms lose (gain) electrons with the majority (minority) spin. In the PDOS curve in Fig. 4(a), this is reflected by the purge of Fe t_{2g} holes in the majority spin channel by the presence of Ge.

Furthermore, the presence of Ge atoms strong reduces magnetic moment of their nearest neighbors. For example, the magnetic moment of Fe_1 atom is reduced to $1.53\mu_B$ in $Fe_{0.75}Ge_{0.25}$, whereas the magnetic moment of the second-neighbor Fe is enhanced to $2.55\mu_B$.

IV. CONCLUSION REMARKS

In summary, we investigated the magnetostriction of $Fe_{1-x}Ge_x$ through extensive FLAPW calculations. Excellent agreement between theory and experiment has been achieved, which indicates the power of density functional approach for studies of magnetostriction. Following a linear increase with the Ge concentration, the magnetostriction rapidly decreases from $x=11\%$ to a large negative value at $x=25\%$. While the lattice softening is important for the initial linearly increase in $\lambda_{001}(x)$, the change in magnetoelastic coupling is responsible to the rapid drop of $\lambda_{001}(x)$ at high concentrations. The electronic origin unraveled through discussions on density of states, spin-orbit coupling interactions and charge density is important for the design of new smart materials.

ACKNOWLEDGMENTS

We would like to thank A. E. Clark, K. B. Hathaway, and T. Lograsso for stimulating discussions. D. Wu is also acknowledged for sending us the experimental data for comparison. Work is supported by the ONR (Grant No. N00014-08-1-0143) and NSF (Grant No. DMR-0706503). Calculations are performed on DOD supercomputers at NAVO, ARSC, and ERDC.

[1] A. E. Clark, in *Ferromagnetic Materials*, edited by E. P. Wohlfarth (North-Holland, Amsterdam, 1980), Vol. 1, Chap. 3.
[2] *Handbook of Giant Magnetostrictive Materials*, edited by G. Engdahl (Academic, San Diego, 2000).
[3] R. Grossinger, R. Sato Turtelli, N. Mehmood, S. Heiss, H. Muller, and C. Bormio-Nunes, J. Magn. Magn. Mater. **320**, 2457 (2008).
[4] A. E. Clark, J.-H. Yoo, J. R. Cullen, M. Wun-Fogle, G. Petculescu, and A. Flatau, J. Appl. Phys. **105**, 07A913 (2009).
[5] G. Petculescu, K. B. Hathaway, T. A. Lograsso, M. Wun-Fogle, and A. E. Clark, J. Appl. Phys. **97**, 10M315 (2005).
[6] A. E. Clark, J. B. Restorff, M. Wun-Fogle, D. Wu, and T. A. Lograsso, J. Appl. Phys, **103**, 07B310 (2008).
[7] D. Wu, Q. Xing, R. W. McCallum, and T. A. Lograsso, J. Appl. Phys. **103**, 07B307 (2008).
[8] G. Petculescu, J. B. LeBlanc, M. Wun-Fogle, J. B. Restorff, D. Wu, T. A. Lograsso, and A. E. Clark (to be published).
[9] R. C. Hall, J. Appl. Phys. **30**, 816 (1959).
[10] A. E. Clark, M. Wun-Fogle, J. B. Restorff, T. A. Lograsso, and G. Petculescu, J. Appl. Phys. **95**, 6942 (2004).
[11] S. C. Hong, W. S. Yun, and R. Wu, Phys. Rev. B **79**, 054419 (2009).
[12] E. M. Summers, T. A. Lograsso, and M. Wun-Fogle, J. Mater. Sci. **42**, 9582 (2007).
[13] A. E. Clark, M. Wun-Fogle, J. B. Restorff, K. W. Dennis, T. A. Lograsso, and R. W. McCallum, J. Appl. Phys. **97**, 10M316 (2005).
[14] G. D. Liu, L. B. Liu, Z. H. Liu, M. Zhang, J. L. Chen, J. Q. Li, G. H. Wu, Y. X. Li, J. P. Qu, and T. S. Chin, Appl. Phys. Lett. **84**, 2124 (2004).
[15] M. C. Zhang, H. L. Jiang, X. X. Gao, J. Zhu, and S. Z. Zhou, J. Appl. Phys. **99**, 023903 (2006).
[16] A. E. Clark, K. B. Hathaway, M. Wun-Fogle, J. B. Restorf, T. A. Lograsso, V. M. Keppens, G. Petculescu, and R. A. Taylor, J. Appl. Phys. **93**, 8621 (2003).
[17] R. Q. Wu, J. Appl. Phys. **91**, 7358 (2002).
[18] S. Pascarelli, M. P. Ruffoni, R. Sato Turtelli, F. Kubel, and R. Grössinger, Phys. Rev. B **77**, 184406 (2008).
[19] M. P. Ruffoni, S. Pascarelli, R. Grössinger, R. S. Turtelli, C. Bormio-Nunes, and R. F. Pettifer, Phys. Rev. Lett. **101**, 147202 (2008).
[20] S. Bhattacharyya, J. R. Jinschek, A. Khachaturyan, H. Cao, J. F.

Li, and D. Viehland, Phys. Rev. B **77**, 104107 (2008).
[21] Q. Xing and T. A. Lograsso, Appl. Phys. Lett. **93**, 182501 (2008).
[22] E. Wimmer, H. Krakauer, M. Weinert, and A. J. Freeman, Phys. Rev. B **24**, 864 (1981).
[23] M. Weinert, E. Wimmer, and A. J. Freeman, Phys. Rev. B **26**, 4571 (1982).
[24] J. P. Perdew, K. Burke, and M. Ernzerhof, Phys. Rev. Lett. **77**, 3865 (1996).
[25] R. Q. Wu and A. J. Freeman, J. Magn. Magn. Mater. **200**, 498 (1999).
[26] R. Q. Wu, L. J. Chen, A. Shick, and A. J. Freeman, J. Magn. Magn. Mater. **177-181**, 1216 (1998).
[27] *Binary Alloy Phase Diagrams*, edited by T. B. Massalski (ASM International, Materials Park, OH, 1990), p. 1706.
[28] G. Ghosh and G. B. Olson, Acta Mater. **50**, 2655 (2002).
[29] R. Zuberek, K. Fronc, W. Paszkowicz, and H. Szymczak, J. Magn. Magn. Mater. **283**, 28 (2004).
[30] Without having Ge first neighborhood, the number of Fe-Ge bonds is $8N_{Ge}$, where N_{Ge} is the number of Ge atoms. If each Fe has only one Fe-Ge bond, we have $N_{Fe}=N-N_{Ge}=8N_{Ge}$, which makes $x=N_{Ge}/N=0.111$.
[31] D. S. Wang, R. Q. Wu, and A. J. Freeman, Phys. Rev. B **47**, 14932 (1993).